Bascule nanobridges self-assembled with ZnO nanowires as double Schottky barrier UV switches

2010 Nanotechnology 21 295502

(http://iopscience.iop.org/0957-4484/21/29/295502)

Nanotechnology **21** (2010) 295502 (7pp) doi:10.1088/0957-4484/21/29/295502

Bascule nanobridges self-assembled with ZnO nanowires as double Schottky barrier UV switches

Yanbo Li[1], **Alexander Paulsen**[1], **Ichiro Yamada**[1], **Yasuo Koide**[2] and **Jean-Jacques Delaunay**[1]

[1] Department of Mechanical Engineering, The University of Tokyo, 7-3-1 Hongo, Bunkyo-ku, Tokyo 113-8656, Japan
[2] Advanced Materials Laboratory, National Institute for Materials Science (NIMS), 1-1 Namiki, Tsukuba, Ibaraki 305-0044, Japan

E-mail: jean@mech.t.u-tokyo.ac.jp

Received 2 March 2010, in final form 3 April 2010
Published 5 July 2010
Online at stacks.iop.org/Nano/21/295502

Abstract
We report the fabrication of a double Schottky barrier (DSB) device by self-assembly of nanowires (NWs). The operating principle of the device is governed by the surface depletion effects of the NWs. High DSBs were formed at the contact interface of ZnO NWs self-assembled into bascule nanobridge (NB) structures. The bascule NB structures exhibited high sensitivity and fast response to UV illumination, having a photocurrent to dark current ratio $>10^4$ and a recovery time as short as $\sim$3 s. The enhanced UV photoresponse of the bascule NB structure is ascribed to the DSB, whose height is tunable with UV light, being high ($\sim$0.77 eV) in dark and low under UV. The bascule NB structure provides a new type of optical switch for spectrally selective light sensing applications ranging from environmental monitoring to optical communication.

(Some figures in this article are in colour only in the electronic version)

1. Introduction

Semiconductor nanowires (NWs) are considered to be ideal building blocks for future nanoscale devices due to their high aspect ratios, good crystal quality, and unique electronic and optical properties [1–3]. So far, semiconductor NWs have been integrated into a wide range of nanoscale devices such as field-effect transistors (FETs) [4–6], p–n junctions [7, 8], nanolasers [9], light-emitting diodes [10, 11], and photodetectors [12–14]. Although functional devices based on semiconductor NWs have already been demonstrated, the full potential of NWs is currently being limited by the effects of surface depletion [15–18]. Surface depletion causing band bending near a semiconductor surface comes as a result of charge trapping by surface states such as dangling bonds, surface defects, and immobile adsorbed ions [19, 20]. Due to the cylindrical geometry and high surface-to-volume ratio of NWs, the surface depletion layer penetrates deep into the NWs. Therefore the performance of the NW devices, in which the carriers are transported along the NW axis, is greatly affected by surface depletion. For example, in NW FETs the carrier mobility is decreased due to the presence of the surface depletion layer [16]. In NW photodetectors, the photogenerated electrons and holes are spatially separated in the NWs due to surface depletion [12, 13, 21, 22]. Although the surface depletion enhances the photoconductive gain [13], it is always associated with a slow photocurrent recovery. These undesirable effects of surface depletion lead to performance degradation of NW devices.

It is the purpose of this paper to show that surface depletion can be beneficial to NW devices, when surface depletion lies at the basis of the operating principle of the device. A proof of concept is presented with ZnO NWs self-assembled into bascule nanobridges (NBs), which exhibit a superior photoresponse owing to surface depletion. The bascule NB structure consists of two cross-bridged ZnO NWs creating a junction at which a double Schottky barrier (DSB) is formed due to the surface depletion. Like a real bascule bridge which can be closed and opened by controlling the movable leaf/leaves [23], the ZnO bascule NB can also be turned on and

off, not by physically moving the NWs, but by changing the height of the DSB at the NW junction using UV illumination. The fabricated ZnO bascule NB had a high DSB in dark and a low DSB under UV illumination, which resulted in a low dark current ($\sim 10^{-11}$ A at 1 V), a high photocurrent to dark current ratio ($>10^4$), a relatively noiseless photocurrent, and an extremely fast photocurrent recovery time ($\sim$3 s). The photoresponse mechanism of ZnO bascule NBs was clarified by comparing the photoresponse of the ZnO bascule NBs with the photoresponses of the ZnO bridging NWs and ZnO NW layers. Based on the surface depletion effects of ZnO NWs, the band gap structure of the ZnO bascule NBs was proposed. The zero-bias height of the DSBs in dark was extracted from activation energy plots. It was found that the current recovery time decreases with barrier height. These results demonstrate unique properties of the ZnO bascule NBs for photodetection that benefit from the surface depletion of ZnO NWs.

2. Experimental details

Process of fabricating the ZnO bascule NBs was very simple, as illustrated in figure 1. A free-standing metal mask was used to pattern thin ($\sim$2 nm) Au pads on a quartz substrate by sputtering. The distance between two facing pads was $\sim$100 μm and six pairs of pads were patterned on a 1×1 cm^2 substrate. ZnO NWs were then grown on the substrate by CVD in a vacuum tube furnace. A 0.30 g powder mixture of ZnO and graphite (2:1 in weight) was used as the source material and located at the center of the furnace. The substrate was placed 5 cm away from the source and downstream of the carrier gases. Argon and oxygen with a ratio of 3:2 were used as the carrier gases at a working pressure of $\sim$50 mbar. The temperature of the furnace was kept at 1000 °C for 30 min and then cooled down naturally. ZnO NW layers were grown selectively on top of the Au pads, while the ZnO bascule NBs were formed in the gap between the ZnO NW layers. For the fabrication of ZnO bridging NWs, the amount of source material was increased to 0.36 g, while the other CVD conditions were kept the same. The scanning electron microscope (SEM) images of the fabricated nanostructures were taken with a Hitachi S-4800.

The time-dependent photoresponse was measured in a tailor-made cell fitted with a gas inlet/outlet, a quartz window, and electrical feedthroughs. The sample was installed in the cell and the ZnO NW layers were contacted with Al probes because Al is known to form a good ohmic contact with ZnO [24]. It is noted that the Au pads formed discontinuous layers and cannot serve as electrodes. Instead, the ZnO NW layers were used as native electrodes to measure the electrical properties of the ZnO bascule NBs. The resistance of the ZnO NW layers was several orders lower than that of the ZnO bascule NBs, so that the voltage drop on the ZnO NW layers can be neglected. Before the measurement, the cell was sealed and filled with dry air since water vapor is known to greatly affect the results [25]. The sample was illuminated through the quartz window by 365 nm UV light filtered from a mercury arc lamp. The UV irradiance was measured by an optical power meter (Ophir PD300-UV). The current was measured with a picoammeter (Keithley 6487). The spectral photoresponse of the ZnO bascule NBs was measured using a spectrophotometer (Jasco V-650) as the light source and the wavelength was scanned from 800 to 200 nm at a rate of 100 nm min^{-1}. The I–V curves were measured with the Keithley 6487 picoammeter by sweeping the voltage from a low to a high value.

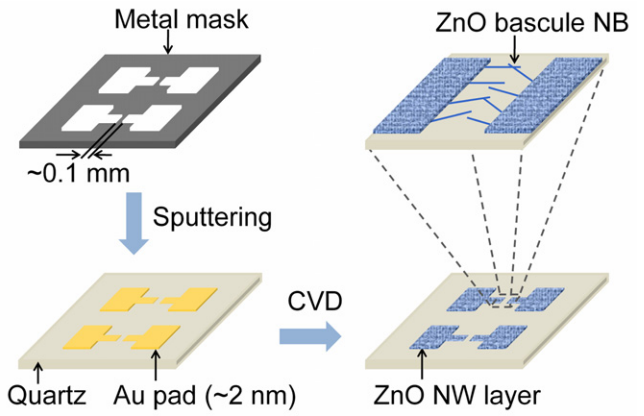

Figure 1. Schematic of the fabrication process. Thin Au pads with a thickness of $\sim$2 nm were sputtered on a quartz substrate through a metal mask. The thin Au pads consist of discontinuous Au particles and are therefore non-conductive. ZnO NW layers were then grown selectively on the Au pads by CVD. ZnO bascule NBs were self-assembled in the gap between the ZnO NW layers.

3. Results and discussion

Figure 2 shows representative SEM images of the ZnO bascule NB structures. As shown in figure 2(a), the ZnO NW layers with a thickness of several tens of micrometers were grown selectively on top of the Au pads on the quartz substrate. Selective growth of ZnO NW layers was achieved due to the low surface energy of quartz [26] and the strong binding affinity of Au to ZnO [27]. The Au particles served as the nucleation sites for the growth of ZnO NWs and remained at the root of the NWs [28]. This is clear from the following observations: Au particles were not found at the tip of the NWs and the thin Au pads could be seen on the substrate after dissolving ZnO NWs in dilute HCl. The gap between the ZnO NW layers is shown in figure 2(b). ZnO NWs (30–50 μm in length) grew laterally from the edge of the ZnO NW layers towards the other side of the gap. A bascule NB was formed when one NW came in contact with another NW growing from the opposite side. The formation of ZnO bascule NBs was a self-assembly process. The number of ZnO bascule NBs formed across the gap was usually four to eight in our experiments. Two ZnO bascule NBs formed in the gap are shown in figure 2(c). Magnified views of the two ZnO bascule NBs in figures 2(d) and (e) show that the ZnO NWs having a diameter of $\sim$100 nm were just in contact with each other. Therefore, the ZnO bascule NB structures should have very high contact barriers at the NW junctions.

The termination of the growth of ZnO upon formation of the ZnO bascule NBs is crucial for the realization of this

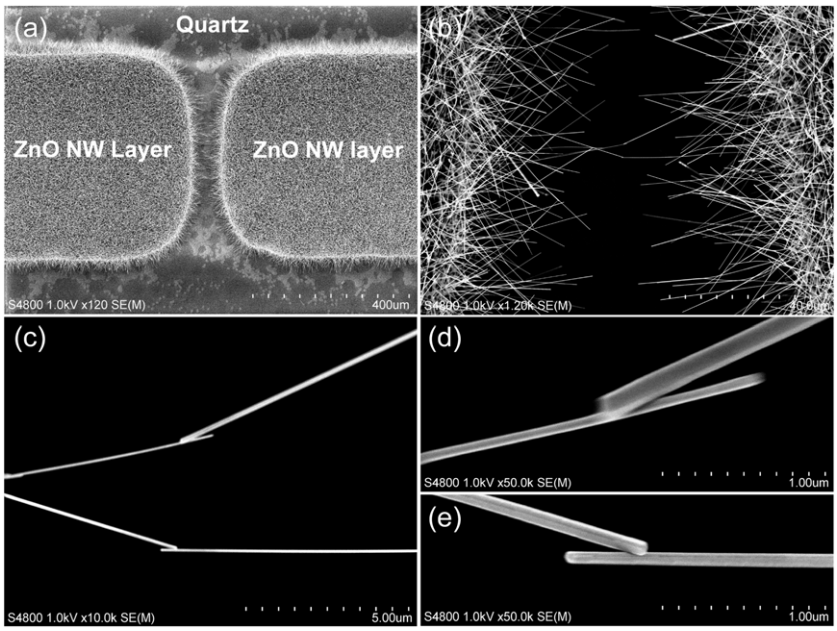

Figure 2. The ZnO bascule NBs obtained by using 0.30 g of source material for the CVD. (a) A SEM image of the gap between the ZnO NW layers. The ZnO NW layers grew selectively on the Au-patterned areas of the substrate. (b) A close-up of the gap showing that ZnO NWs at the edges of the layers grew towards the opposite layers and ZnO bascule NBs were formed in the gap. (c) Magnified view of two ZnO bascule NBs. Close-ups of the two ZnO bascule NBs are shown in (d) and (e).

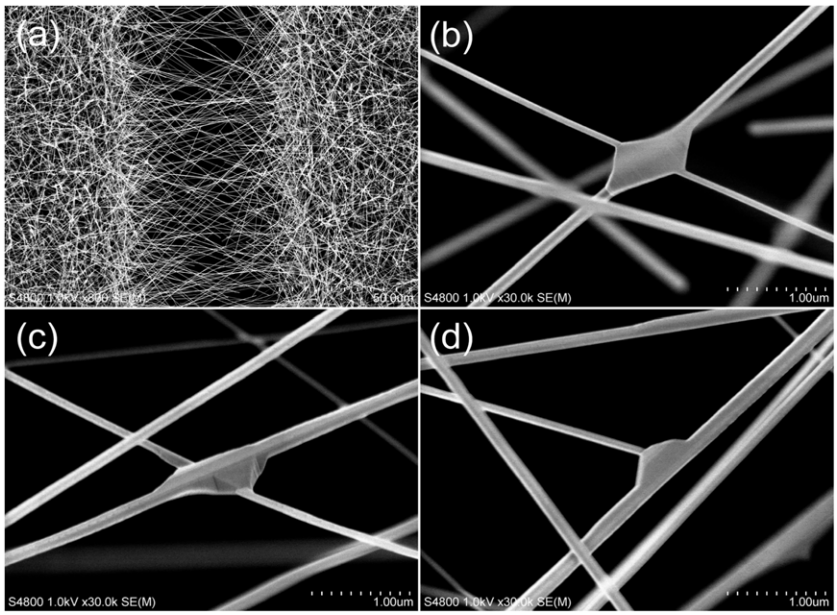

Figure 3. The ZnO bridging NWs obtained by using 0.36 g of source material for the CVD. (a) A SEM image of the ZnO bridging NWs in the gap between the ZnO NW layers. (b)–(d) Magnified views of the bridging NWs in the gap reveal that ZnO grew at the NW junctions and fused the NWs.

structure. Control of the growth termination is achieved by precisely controlling the amount of source material used in the CVD process. If the amount of source material was insufficient, the ZnO NWs were too short to form any bascule NBs. In contrast, when the amount of source material was too great, the ZnO NWs grew long enough to cross the gap and form bridges directly. Figure 3(a) shows ZnO bridging NWs obtained from 0.36 g of source material. This large amount of source material allows for the growth to continue after the formation of ZnO bascule NBs. ZnO then nucleates at the NW junctions and fuses the NWs, as shown in figures 3(b)–(d). The contact barriers of these fused NWs should therefore be reduced when compared with bascule NBs.

Figure 4(a) shows the time-dependent photoresponse of the ZnO bascule NBs. Under a bias voltage of 1 V, the dark current was only $\sim 10^{-11}$ A. The current increased by more than four orders of magnitude under an irradiance of ~ 0.8 mW cm^{-2}. Besides the drastic increase in current, the

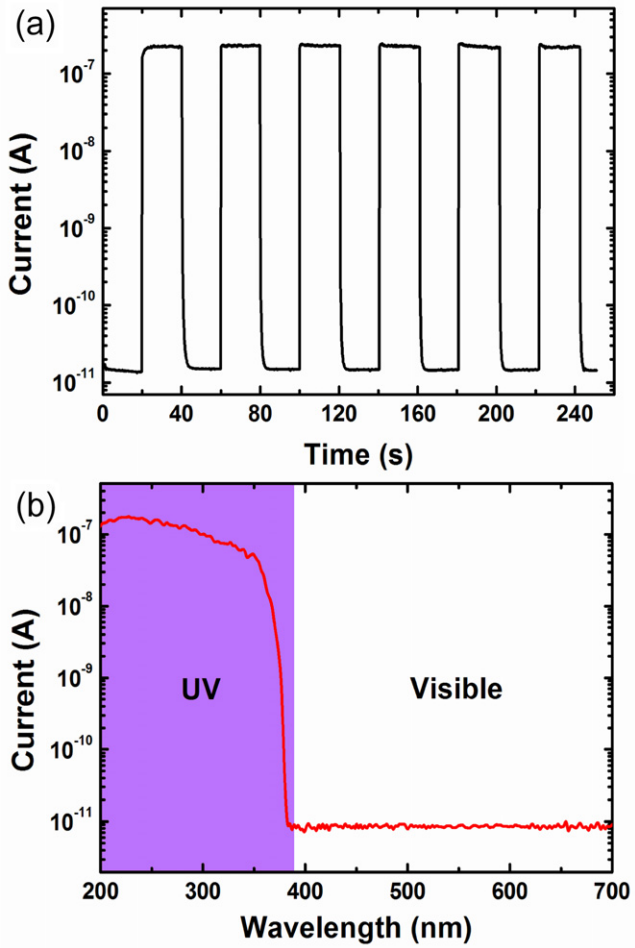

Figure 4. (a) The photoresponse of the ZnO bascule NBs when illuminated with 20 s pulses of UV light in dry air. The bias voltage was 1 V and the UV irradiance was ∼0.8 mW cm^{-2}. (b) The spectral photoresponse of the ZnO bascule NBs, exhibiting a sharp cut-off wavelength at ∼380 nm.

noise in the photocurrent was very low. More importantly, the current recovery after switching off the UV light was extremely fast. The recovery time (defined as the time needed to fully recover to the dark level) was only ∼3 s. To put this into context, the recovery time of ZnO NW photoconductive detectors is generally in the range of hundreds to thousands of seconds [13, 21, 22]. The recovery time of the ZnO bascule NBs was even shorter than that of the reported ZnO NW metal–semiconductor–metal (MSM) [14] and Schottky barrier photodetectors [29]. As shown in figure 4(b), the current was insensitive to visible light and increased sharply by ∼4 orders of magnitude at ∼380 nm. The photon energy for the onset of the current corresponds to the band gap energy of ZnO (∼3.3 eV). The high spectral selectivity in combination with low operating voltage, low dark current, high photocurrent to dark current ratio, low-noise photocurrent, and fast response and recovery, demonstrate that ZnO bascule NBs are ideal building blocks for the design of novel UV photodetectors.

To clarify the origin of the extremely fast photocurrent recovery process of the ZnO bascule NBs, the photoresponse of the ZnO bascule NBs was compared with the photoresponses

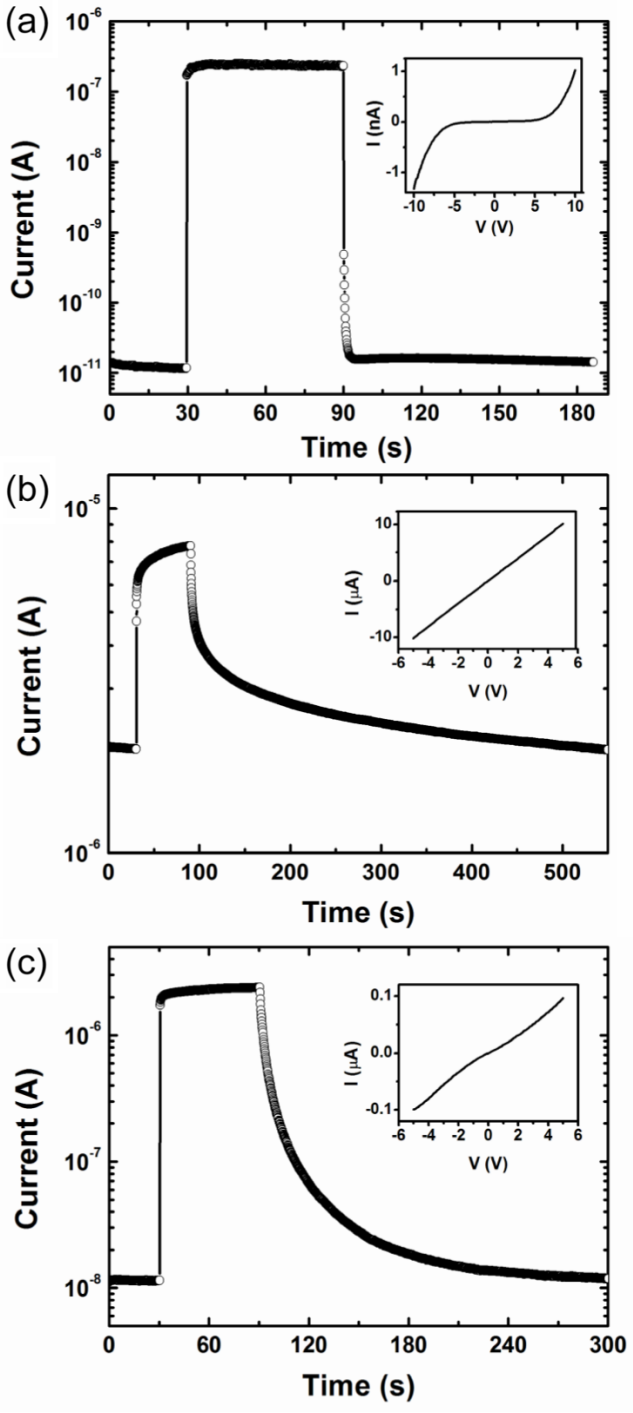

Figure 5. Time-dependent photoresponse of (a) the ZnO bascule NBs, (b) the ZnO NW layer, and (c) the ZnO bridging NWs. The photocurrent decay time and recovery time are (a) ≪0.12 and ∼3 s, (b) ∼82 and ∼460 s, and (c) ∼2.4 and ∼210 s. The measurements were carried out in dry air under 1 V bias voltage and ∼0.8 mW cm^{-2} UV illumination. The insets show the corresponding I–V curves measured in the dark.

of the ZnO NW layer and ZnO bridging NWs. The photoresponses together with their I–V curves under dark conditions of the three different structures are presented in figure 5. Although the three structures were all made of the same ZnO NWs, the difference in the structures resulted

in drastic changes in the UV photoresponses and dark I–V curves. The time-dependent photoresponse of the ZnO bascule NBs in figure 5(a) reveals a current decrease upon switching off UV light of more than two orders of magnitude between two consecutive measurement points (corresponding to a sampling interval of 0.12 s). The decay time, defined as the time needed to recover to $1/e$ (∼36.8%) of the maximum photocurrent, was therefore much shorter than 0.12 s. Furthermore, the recovery time was only ∼3 s. The dark I–V curve of the ZnO bascule NBs is highly nonlinear and nearly symmetrical with respect to the applied voltage, as seen in the inset of figure 5(a). These I–V characteristics are typically obtained for DSBs and semiconductor grain boundaries [30–34]. The highly nonlinear I–V curve of figure 5(a) indicates high potential barriers in the structure. The potential barriers may have three origins: the barriers at the two Al/ZnO contacts, the barriers within the ZnO NW layers, and the barriers at the NW junctions of the ZnO bascule NBs. However, the dark I–V curve of the ZnO NW layer measured using the same Al probes is linear, as seen in the inset of figure 5(b). This strongly suggests that the potential barriers at the two Al/ZnO contacts and within the ZnO NW layer are negligible. It is therefore concluded that the potential barriers arose mainly from the NW junctions of the ZnO bascule NBs. Figure 5(b) shows the time-dependent photoresponse of the ZnO NW layers. Along with the linear I–V curve, a very slow current recovery process was observed for the ZnO NW layer with negligible barriers. The decay time and the recovery time were ∼82 s and ∼460 s, respectively. Therefore, the high potential barriers at the NW junctions should account for the fast current recovery process of the ZnO bascule NBs. This is further evidenced by the photoresponse and dark I–V curve of the ZnO bridging NWs. Due to the growth of ZnO at the NW junctions (see figures 4(b)–(d), low potential barriers were formed in the ZnO bridging NWs, as reflected by the slight bend in the dark I–V curve of figure 5(c). Consequently, a decay time of ∼2.4 s and a recovery time of ∼210 s were obtained, which were much longer than those of the ZnO bascule NBs with high barriers but much shorter than those of the ZnO NW layers with negligible barriers. These results demonstrated that the current recovery process was greatly influenced by the potential barriers in the structures. The higher the potential barrier, the faster the current recovery. The extremely fast current recovery observed in the photoresponse of the ZnO bascule NBs was explained by the high potential barriers at the NW junctions of the ZnO bascule NBs.

Figure 6 shows a schematic diagram of the ZnO bascule NB, together with the energy band gap diagrams of the ZnO NW and the DSB at the NW junction in the dark. It is known that in the dark oxygen molecules became adsorbed on the surface of the ZnO NW, capturing free electrons in the n-type NW and creating a high density of surface trap states [12, 13]. The NW surface becomes negatively charged, which results in upward band bending of the energy bands, as illustrated in the top left diagram of figure 6. When a bascule NB is formed, a DSB arises at the NW junction due to the band bending in the NWs and the high density of trap states at the boundary of the NW junction. Under zero applied voltage, the barrier heights on both sides are the same. Application of a voltage causes the barrier to decrease slightly in the negative NW, but to increase considerably in the more positive NW (top right diagram of figure 6). When ZnO NWs are illuminated by UV light, the surface trap states are filled by photogenerated holes and the oxygen molecules are desorbed from the NW surface. The energy bands in the NWs become less bent. Similarly, when the ZnO bascule NBs are illuminated by UV light, the trap states at the boundary of the NW junction are filled by holes and the height of the DSB is decreased.

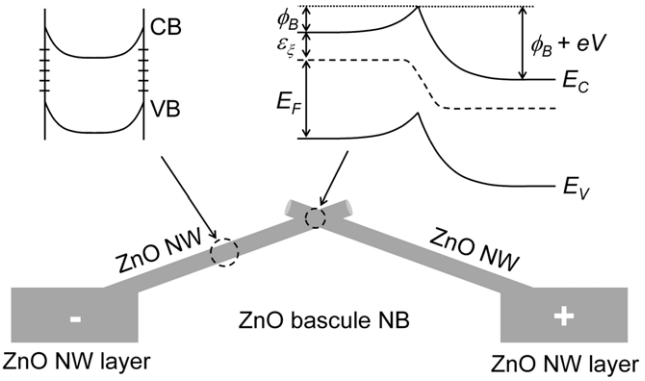

Figure 6. Schematic of the ZnO bascule NB (bottom). The top left schematic represents the energy band gap of the ZnO NW in the dark, indicating surface trap states causing band bending of the conduction band (CB) and the valence band (VB). The top right diagram shows the energy band gap of the DSB at the boundary of the NW junction under a bias voltage V in the dark.

The role of the DSBs in the photoresponse of the ZnO bascule NBs can be clarified as follows. In the dark, electrons have to overcome the high DSBs at the NW junctions, which results in a very low dark current. The ZnO bascule NBs are in an 'off-state' in the dark. They can be turned to an 'on-state' by UV light, because the height of the DSBs is decreased under UV illumination. In the 'on-state', the photogenerated carriers can easily cross the barriers and give rise to a high photocurrent. The decrease in the barrier height under UV illumination also produces a low-noise photocurrent, in contrast to the high-noise photocurrent of Schottky-type photodetectors such as the Pt/ZnO NW [29], Au/Cr/ZnS NW [35], and Au/Ga_2O_3 NW [36] with high Schottky barriers. The photocurrent noise of a Schottky barrier photodetector is ascribed to the fluctuation of the potential barriers that controls the electron injection from the metal electrodes into the conduction band of the photoconducting materials [37]. The large fluctuation of the potential barrier in these Schottky photodetectors results in a high-noise photocurrent, while in the bascule NB photodetector the potential barrier is very low under UV illumination and the small fluctuation accounts for the low-noise photocurrent. After switching off the UV light, the ZnO bascule NBs return to the 'off-state' again. The barrier height is increased by the re-adsorption of oxygen molecules at the boundary of the NW junctions. The current decreases rapidly to the dark level owing to the high potential barriers. The current recovery process of ZnO NW photoconductors is slow because the electrons are confined to the core of the

NWs due to the upward band bending, so that the electrons cannot be captured easily by adsorbed oxygen molecules at the surface [13, 25]. On the contrary, in the ZnO bascule NBs the electrons have to cross the boundary with high trap states, where they have a high probability of being captured.

The NW–boundary–NW structure in the ZnO bascule NBs can be treated as a single grain boundary structure: the ZnO NWs are the single crystalline grains and the NW junction is the grain boundary. Thermionic emission is believed to be the dominant mechanism for carrier transport through the DSB at a grain boundary under dark conditions [30–34]. The thermionic emission current is given by:

$$I = SA^*T^2 \exp\left(-\frac{\phi_B + \varepsilon_\xi}{k_B T}\right)\left[1 - \exp\left(-\frac{eV}{k_B T}\right)\right] \quad (1)$$

where S is the area of the boundary, A^* is the Richardson constant, T is the temperature, ϕ_B is the barrier height, ε_ξ is the Fermi level measured from the conduction band, k_B is the Boltzmann constant, and V is the bias voltage. The zero-bias conductance G_0 is obtained from equation (1):

$$G_0 = \lim_{V\to 0}\frac{I}{V} = SA^*\frac{eT}{k_B}\exp\left(-\frac{\phi_{B0} + \varepsilon_\xi}{k_B T}\right) \quad (2)$$

where $\phi_{B0} \equiv \phi_B(V = 0)$. Since G_0 can be obtained experimentally, the activation energy E_{act} is deduced from:

$$E_{act} \equiv -k_B\frac{\partial \ln G_0}{\partial(1/T)} \simeq \phi_{B0} + \varepsilon_\xi. \quad (3)$$

Figure 7(a) shows the activation energy plots of the three structures studied in figure 5. The G_0 values in figure 7(a) were obtained in the temperature range of 300–400 K from the slopes of the I–V curves measured under small bias voltage (0–0.1 V) in dark. The activation energies were obtained from the slopes of the linear fits in figure 7(a) using equations (3). The activation energies of the ZnO bascule NBs, the ZnO bridging NWs, and the ZnO NW layer were 0.96, 0.31, and 0.19 eV, respectively. E_{act} is approximately equal to $\phi_{B0} + \varepsilon_\xi$, since ϕ_{B0} and ε_ξ are essentially temperature independent in the measured temperature range [38]. Moreover, ε_ξ is generally very small in ZnO [33] so higher activation energy corresponds to higher potential barriers in the studied structures.

In the ZnO bascule NBs, the barriers originate from the Al/ZnO contacts, the ZnO NW layers, and the NW junctions of the NBs. However, in the ZnO NW layer the barriers are from the Al/ZnO contacts and the ZnO NW layer. Therefore, by subtracting the E_{act} of the ZnO bascule NBs from that of the ZnO NW layer, the ϕ_{B0} of the DSBs at the NW junctions of the ZnO bascule NBs is estimated to be 0.77 eV. Similarly, the ϕ_{B0} of the ZnO bridging NWs can be estimated to be 0.12 eV. Using equation (2), equation (1) can be rewritten as:

$$I = \frac{G_0 k_B T}{e}\exp\left(\frac{\phi_{B0} - \phi_B}{k_B T}\right)\left[1 - \exp\left(-\frac{eV}{k_B T}\right)\right]. \quad (4)$$

Solving for ϕ_B leads to:

$$\phi_B = \phi_{B0} - k_B T \ln\left\{\frac{eI}{k_B T G_0}\left[1 - \exp\left(-\frac{eV}{k_B T}\right)\right]^{-1}\right\}. \quad (5)$$

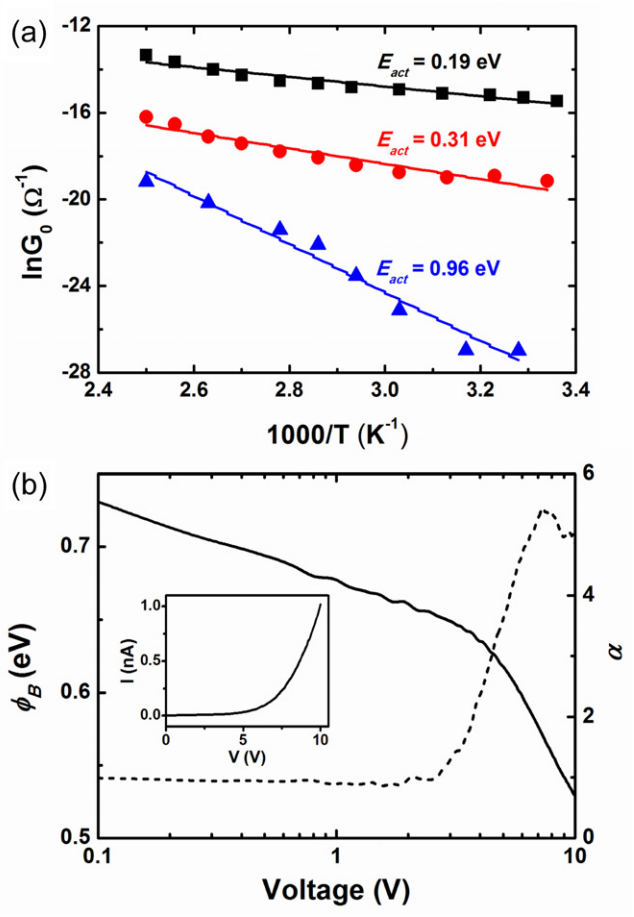

Figure 7. (a) Activation energy plots of the ZnO bascule NBs (blue triangles), the ZnO bridging NWs (red circles), and the ZnO NW layer (black squares). The lines are the linear fits to the experimental data, from which the corresponding activation energies E_{act} are calculated. (b) The barrier height ϕ_B (solid line) and the nonlinearity coefficient α (dashed line) versus bias voltage for the ZnO bascule NBs, as calculated from the I–V curve shown in the inset.

Using equation (5) and the I–V curves measured in the dark, the variation in the barrier height with the bias voltage is plotted in figure 7(b) for the ZnO bascule NBs. It is found that the barrier height decreases gradually until a bias voltage of ∼3 V, and then sustains an abrupt decrease above 3 V. The decrease in the barrier height with bias voltage is ascribed to the filling of the interface trap states [33]. To quantify the breakdown behavior of the bascule NBs, the nonlinearity coefficient $\alpha = \mathrm{d}(\ln I)/\mathrm{d}(\ln V)$ is also shown in figure 7(b). Under a bias voltage less than 3 V, α is almost constant and equal to ∼1. The drastic increase in α above 3 V indicates that the traps states at the boundary of the NW junctions are rapidly filled at these high bias voltages [33]. This is consistent with the drastic decrease in the barrier height above 3 V. Therefore, the ZnO bascule NBs should be operated at a bias voltage below 3 V to avoid breakdown and achieve fast recovery.

4. Conclusion

In conclusion, we demonstrated that the surface depletion effects in the ZnO NWs could be utilized to realize a unique

bascule NB structure. The ZnO bascule NBs were self-assembled with ZnO NWs in a single-step CVD process. DSBs were formed at the NW junctions of the ZnO bascule NBs owing to the surface depletion effects in the ZnO NWs. Due to the tunable DSB height, which was high in the dark and low under UV illumination, the ZnO bascule NBs could be switched on and off by turning the UV light on and off. As a result, the ZnO bascule NBs exhibited outstanding properties in UV sensing, including low dark current ($\sim 10^{-11}$ A at 1 V), high photocurrent to dark current ratio ($>10^4$), and low-noise photocurrent. More remarkably, the photocurrent recovery process was extremely fast having a recovery time of only $\sim$3 s. The origin of the fast recovery was found to be the high DSBs at the boundary of the NW junctions of the ZnO bascule NBs by comparing the photoresponses of structures with different barrier heights. The zero-bias height of the DSBs was estimated from the activation energy plots to be $\sim$0.77 eV. Also, the range of bias voltage in which the ZnO bascule NBs should be operated to avoid breakdown was obtained by examining the change of the barrier height with the bias voltage. Our results demonstrated that the ZnO bascule NBs provide the ability to detect UV with high sensitivity and fast response. Finally, it is noted that the bascule NB structure can be formed with a large variety of NW materials, consequently widening the range of applications of the bascule NBs to not only spectrally selective light sensors but also gas sensors and biochemical sensors.

Acknowledgments

This work was supported through the Global COE Program, 'Global Center of Excellence for Mechanical Systems Innovation,' and Grants-in-Aid for Scientific Research (B) 22360056 from the Ministry of Education, Culture, Sports, Science and Technology (MEXT), Japan. Part of this work was conducted in Center for Nano Lithography and Analysis, The University of Tokyo, supported by the MEXT, Japan. We thank Shigeo Maruyama and Rong Xiang for SEM characterization and fruitful discussion.

References

[1] Lieber C M and Wang Z L 2007 *MRS Bull.* **32** 99–108
[2] Li Y, Qian F, Xiang J and Lieber C M 2006 *Mater. Today* **9** 18–27
[3] Agarwal A and Lieber C M 2006 *Appl. Phys.* A **85** 209–15
[4] Duan X F, Huang Y, Cui Y, Wang J F and Lieber C M 2001 *Nature* **409** 66–9
[5] Ju S Y, Facchetti A, Xuan Y, Liu J, Ishikawa F, Ye P D, Zhou C W, Marks T J and Janes D B 2007 *Nat. Nanotechnol.* **2** 378–84
[6] Lu W, Xie P and Lieber C M 2008 *IEEE Trans. Electron Devices* **55** 2859–76
[7] Cui Y and Lieber C M 2001 *Science* **291** 851–3
[8] Li P J, Liao Z M, Zhang X Z, Zhang X J, Zhu H C, Gao J Y, Laurent K, Leprince-Wang Y, Wang N and Yu D P 2009 *Nano Lett.* **9** 2513–8
[9] Huang M H, Mao S, Feick H, Yan H Q, Wu Y Y, Kind H, Weber E, Russo R and Yang P D 2001 *Science* **292** 1897–9
[10] Zimmler M A, Stichtenoth D, Ronning C, Yi W, Narayanamurti V, Voss T and Capasso F 2008 *Nano Lett.* **8** 1695–9
[11] Lai E, Kim W and Yang P D 2008 *Nano Res.* **1** 123–8
[12] Li Y B, Della Valle F, Simonnet M, Yamada I and Delaunay J-J 2009 *Nanotechnology* **20** 045501
[13] Soci C, Zhang A, Xiang B, Dayeh S A, Aplin D P R, Park J, Bao X Y, Lo Y H and Wang D L 2007 *Nano Lett.* **7** 1003–9
[14] Kind H, Yan H Q, Messer B, Law M and Yang P D 2002 *Adv. Mater.* **14** 158–60
[15] Leonard F and Talin A A 2006 *Phys. Rev. Lett.* **97** 026804
[16] Motayed A, Vaudin M, Davydov A V, Melngailis J, He M Q and Mohammad S N 2007 *Appl. Phys. Lett.* **90** 043104
[17] Calarco R, Marso M, Richter T, Aykanat A I, Meijers R, Hart A V, Stoica T and Luth H 2005 *Nano Lett.* **5** 981–4
[18] Simpkins B S, Mastro M A, Eddy C R and Pehrsson P E 2008 *J. Appl. Phys.* **103** 104313
[19] Darling R B 1991 *Phys. Rev.* B **43** 4071–83
[20] Garrett C G B and Brattain W H 1955 *Phys. Rev.* **99** 376–87
[21] Li Q H, Gao T, Wang Y G and Wang T H 2005 *Appl. Phys. Lett.* **86** 123117
[22] Ahn S E, Lee J S, Kim H, Kim S, Kang B H, Kim K H and Kim G T 2004 *Appl. Phys. Lett.* **84** 5022–4
[23] Koglin T L 2003 *Movable Bridge Engineering* (New York: Wiley) pp 33–54
[24] Kim H K, Kim K K, Park S J, Seong T Y and Adesida I 2003 *J. Appl. Phys.* **94** 4225–7
[25] Li Y B, Della Valle F, Simonnet M, Yamada I and Delaunay J-J 2009 *Appl. Phys. Lett.* **94** 023110
[26] Shchipalov Y K 2000 *Glass Ceram.* **57** 374–7
[27] Albert-Polaçek K and Wassermann E F 1976 *Thin Solid Films* **37** 65–71
[28] Kim D S, Scholz R, Gösele U and Zacharias M 2008 *Small* **4** 1615–9
[29] Zhou J, Gu Y D, Hu Y F, Mai W J, Yeh P H, Bao G, Sood A K, Polla D L and Wang Z L 2009 *Appl. Phys. Lett.* **94** 191103
[30] Eda K 1978 *J. Appl. Phys.* **49** 2964–72
[31] Mahan G D, Levinson L M and Philipp H R 1979 *J. Appl. Phys.* **50** 2799–812
[32] Pike G E and Seager C H 1979 *J. Appl. Phys.* **50** 3414–22
[33] Blatter G and Greuter F 1986 *Phys. Rev.* B **33** 3952–66
[34] Canessa E and Nguyen V L 1992 *Physica* B **179** 335–41
[35] Fang X S *et al* 2009 *Adv. Mater.* **21** 2034–9
[36] Feng P, Zhang J Y, Li Q H and Wang T H 2006 *Appl. Phys. Lett.* **88** 153107
[37] Carbone A and Mazzetti P 1994 *Phys. Rev.* B **49** 7592–602
[38] Sze S M and Ng K K 2007 *Physics of Semiconductor Devices* 3rd edn (New York: Wiley) p 174